Quantum Gaussian Noise

Jeffrey H. Shapiro

Research Laboratory of Electronics
Massachusetts Institute of Technology
Cambridge, MA 02139-4307

ABSTRACT

In semiclassical theory, light is a classical electromagnetic wave and the fundamental source of photodetection noise is the shot effect arising from the discreteness of the electron charge. In quantum theory, light is a quantum-mechanical entity and the fundamental source of photodetection noise comes from measuring the photon-flux operator. The Glauber coherent states are Gaussian quantum states which represent classical electromagnetic radiation. Quantum photodetection of these states yields statistics that are indistinguishable from the corresponding Poisson point-process results of semiclassical photodetection. Optical parametric interactions, however, can be used to produce other Gaussian quantum states, states whose photodetection behavior cannot be characterized semiclassically. A unified analytical framework is presented for Gaussian-state photodetection that includes the full panoply of nonclassical effects that have been produced via parametric interactions.

Keywords: Coherent states, squeezed states, photon twins, polarization entanglement, parametric amplifiers

1. INTRODUCTION

High-sensitivity photodetectors are in widespread use in high-performance optical communication and interferometric precision-measurement systems. Statistical analyses of such systems almost invariably rely on the semiclassical theory of photodetection.[1–3] According to semiclassical theory, light is a classical electromagnetic wave whose absorption, by a photodetector, creates charge carriers (usually hole-electron pairs in the depletion region of a back-biased semiconductor junction) that can be sensed in an external circuit. The assumption that, under quiescent (constant-power) illumination conditions, these charge carriers are created instantaneously in a Poisson point-process manner then leads to the fundamental shot-noise sensitivity limit of the semiclassical theory. Light, however, is a quantum-mechanical entity, whose photodetection statistics depend on its quantum state.[4, 5] In other words, the noise seen in high-sensitivity photodetection systems is not shot noise; it is the quantum noise of the light beam itself.

Lasers, light-emitting diodes, and incandescent sources all produce light beams that are in Glauber coherent states or their classically-random mixtures.[6] In photodetection analyses these quantum states are said to be classical, because their quantum-photodetection statistics agree exactly with those of the semiclassical theory.[4, 5] It is possible, however, to produce light-beam quantum states whose photodetection statistics cannot be obtained from semiclassical theory. The quantum-photodetection behavior of these states has been seen in experiments that have produced quadrature-noise squeezing,[7] photon-twin beams,[8] nonclassical fourth-order interference,[9] and polarization entangled photon pairs.[10] Nonclassical states offer new application possibilities—low-insertion-loss, constant signal-to-noise-ratio waveguide taps,[11] sub-shot-noise sensitivity interferometers,[12] entanglement-based quantum cryptography,[13] and quantum teleportation[14, 15]—that are impossible within the framework of semiclassical photodetection.

The Glauber coherent states are Gaussian states: their wave functions are Gaussian.[6] So too are the states employed in squeezing, photon twins, nonclassical fourth-order interference, and polarization entanglement experiments..[16, 17] This paper is devoted to their study, i.e., to quantum Gaussian noise. We begin by contrasting the semiclassical and quantum theories of photodetection. We then present a physical model for the generation of quantum Gaussian noise, viz., the optical parametric amplifier. Using this model, we build a unified framework for all of the preceding nonclassical photodetection effects.

Send correspondence to J. H. Shapiro, E-mail: jhs@mit.edu, Telephone: 617-253-4179.

2. SEMICLASSICAL VERSUS QUANTUM PHOTODETECTION

The distinctions between semiclassical and quantum photodetection arise in connection with the fundamental noise limits seen in optical measurements. It is important, at the outset, to make clear that only high-sensitivity photodetection systems will reach these fundamental noise limits. In Fig. 1 we have a block diagram showing the essential features of a real photodetection system. A real photodetector has an implicit optical filter, representing
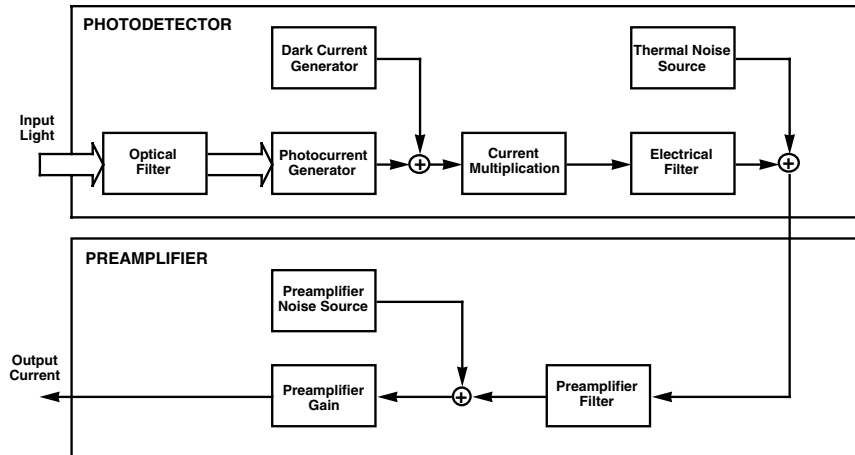

Figure 1. Block diagram of a real photodetection system showing the primary sources of noise in the detector and the subsequent preamplifier. Optical signals are shown as wide arrows; electrical signals are shown as thin arrows.

the wavelength sensitivity of its photoabsorption process, and an implicit electrical filter, imposing a bandwidth limit on its output current. The fundamental core of the detection system is its photocurrent generator, where instantaneous production of charge carriers occurs in response to illumination. A real photodetector also has dark current, arising from leakage and other non-illumination related sources. It may employ current multiplication—such as avalanche gain in a semiconductor photodiode or secondary-electron multiplication in a photomultiplier tube—to magnify the photocurrent prior to its immersion in the thermal noise associated with the detector's resistive load. Because the output current from a real photodetector may not be sufficient to ignore the noise levels in subsequent electronic circuits, the bandwidth, gain, and noise of the first preamplifier should be included in a complete photodetection sensitivity analysis.

In all that follows we shall strip away every element of Fig. 1 except the photocurrent generator. For quasimonochromatic (narrowband) illumination of a detector whose dark current is very low and whose internal current multiplication is very high (and noise free) this is a reasonable approximation. Photomultiplier tubes typically meet these conditions. Alternatively, when coherent mixing is performed, i.e., optical homodyne or heterodyne detection,[1] even a zero-internal-gain semiconductor photodiode can yield an output current whose noise behavior is well characterized by this approximation.

The ideal photodetection system we shall consider is shown in Fig. 2 and its current and counting waveforms are sketched in Fig. 3. A quasimonochromatic light beam illuminates the detector, producing a photocurrent,
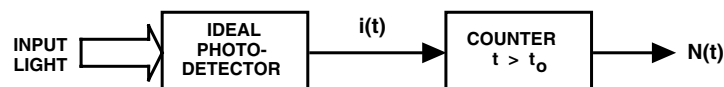

Figure 2. Block diagram of an ideal photodetection system.

$i(t)$, that is a train of charge-q impulses located at carrier-generation occurrence times $\{t_i\}$. This impulse train drives a counting circuit, initiated at time $t = t_0$, to produce a counting process, $N(t)$, which increments by one at each occurrence time. Note that we have yet to make any distinction between semiclassical and
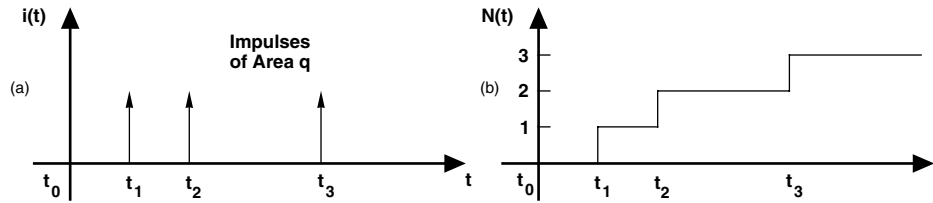
Figure 3. Left (a), photocurrent impulse train. Right (b), photocount process.

quantum photodetection. That will come in the next two subsections, when we instantiate the statistics of the photocurrent-generation block.

2.1. Semiclassical Photodetection

To keep our presentation at a manageable level of detail, we shall ignore the polarization and spatial dependence of the electromagnetic wave impinging on the ideal photodetector shown in Fig. 2. If that light has center frequency ω rad/s, it can then be characterized by a positive-frequency, complex-field envelope $E(t)$ such that $P(t) \equiv \hbar\omega|E(t)|^2$ is the short-time-average power falling on the sensitive region of the detector at time t. Here, $\hbar$ is Planck's constant divided by 2π, and so $\hbar\omega$ is the photon energy at the source's center frequency. In the semiclassical theory, however, electromagnetic fields are classical and there are no photons. Hence $\hbar\omega$ merely appears, at the moment, as a convenient normalization term.

In general, $E(t)$ is a complex-valued random process, because we seldom have light sources of sufficient purity to regard them as deterministic electromagnetic waves. This randomness, in turn, makes $P(t)$ a non-negative, real-valued random process. The semiclassical theory of photodetection posits a Poisson point process model for the photocurrent, conditioned on knowledge of $P(t)$.[1, 2, 18] Specifically, if $P(t)$ is known for $t \in \mathcal{T}$, then $i(t)$ for $t \in \mathcal{T}$ is a train of area-q impulses, as shown in Fig. 3(a), whose occurrence times, $\{t_i\}$, are an inhomogeneous Poisson point process of rate function $\lambda(t) = P(t)/\hbar\omega$. Strictly speaking, this rate function should include a dimensionless factor of η, where $0 < \eta \leq 1$ is the quantum efficiency of the device. Because we are trying to delineate the limits on ideal photodetection, we have set $\eta = 1$. Photomultiplier tubes do not approach unity quantum efficiency, although semiconductor photodiodes can. The inclusion of sub-unity quantum efficiency in the quantum theory is more complicated than it is in the semiclassical case and the $\eta = 1$ restriction is then non-trivial.[4, 5]

The classical field $E(t)$ has units $\sqrt{\text{photons/sec}}$. Thus, our ideal semiclassical photodetector produces a conditional Poisson impulse train whose rate function is the classical photon flux, $\lambda(t) = |E(t)|^2$, viz., the classical short-time-average power illuminating the detector measured in $\hbar\omega$ units. Photon flux plays a prominent role in the quantum theory of photodetection, hence the normalization choice we have made for the semiclassical case.

2.2. Quantum Photodetection

In the quantum theory of light, with polarization and spatial dependence neglected, the positive-frequency complex envelope $E(t)$ from classical electromagnetics is replaced by a non-Hermitian Hilbert-space operator $\hat{E}(t)$, which annihilates a photon at time t. Its associated adjoint operator, $\hat{E}^\dagger(t)$, creates a photon at time t. The Heisenberg uncertainty principle for the real and imaginary parts of the field, $\hat{E}_1(t) \equiv \text{Re}[\hat{E}(t)]$ and $\hat{E}_2(t) \equiv \text{Im}[\hat{E}(t)]$, then arises from the non-zero commutator

$$\left[\hat{E}(t), \hat{E}^\dagger(u)\right] = \delta(t - u). \tag{1}$$

It is a general tenet of quantum theory that the statistics of an observation depend on the operator representation of the measurement and the state of the quantum system that is being observed.[19] For the Fig. 2 ideal photodetector, the quantum theory of photodetection states that the classical photocurrent, $i(t)$, has the same statistics as the quantum measurement operator $\hat{i}(t) \equiv q\hat{E}^\dagger(t)\hat{E}(t)$, i.e., the charge q times the photon-flux operator $\hat{E}^\dagger(t)\hat{E}(t)$.[4]

Within the preceding framework, the connection between quantum photodetection and semiclassical photodetection is established as follows. The Glauber coherent states are the eigenkets of the field operator $\hat{E}(t)$:

$$\hat{E}(t)|E(t)\rangle = E(t)|E(t)\rangle, \quad \text{for } t \in \mathcal{T}, \tag{2}$$

characterizes a quantum state (ket) vector $|E(t)\rangle$, and its associated classical complex-valued eigenfunction $E(t)$, over the observation interval $\mathcal{T}$. Moreover, when the field is in the coherent state with eigenfunction $E(t)$, the output of the $\hat{i}(t)$ quantum measurement is a train of area-q impulses, as shown in Fig. 3(a), whose occurrence times are a Poisson point process with rate function $\lambda(t) = |E(t)|^2$.[4] So, if the quantum field is in a coherent state $|E(t)\rangle$, or a classically-random mixture of such states, then the quantum theory of photodetection coincides, in all its quantitative statistical predictions, with the semiclassical theory. There is still a fundamental qualitative difference between these theories in that the semiclassical theory ascribes the photodetection noise (when $|E(t)|^2$ is deterministic) to the shot effect, whereas the quantum theory identifies the photodetection noise (when the field is in the state $|E(t)\rangle\rangle$) as the quantum noise of the coherent state manifest through the photon-flux operator measurement. For nonclassical light sources these interpretations diverge in their quantitative predictions, and the quantum theory of photodetection must be employed. Before turning to how nonclassical Gaussian light-beam states can be generated via optical parametric interactions, it will be useful to describe these nonclassical Gaussian states in simple, abstract single-mode terms.

2.3. Coherent States versus Squeezed States

The frequency-ω component of the quantum field $\hat{E}(t)$ over the finite time interval $0 \le t \le T$ is of the form $\hat{a}e^{-j\omega t}/\sqrt{T}$, where the photon annihilation operator $\hat{a}$, and its adjoint (the photon creation operator) $\hat{a}^\dagger$, satisfy the commutator relation $[\hat{a}, \hat{a}^\dagger] = 1$. The coherent states of this single mode, $\{\,|\alpha\rangle : \alpha \in \mathcal{C}\,\}$, are minimum uncertainty-product states for the resulting Heisenberg inequality,

$$\langle[\Delta\hat{a}_1(t)]^2\rangle\langle[\Delta\hat{a}_2(t)]^2\rangle \ge 1/16, \tag{3}$$

where $\hat{a}_1(t) \equiv \mathrm{Re}(\hat{a}e^{-j\omega t})$ and $\hat{a}_2(t) \equiv \mathrm{Im}(\hat{a}e^{-j\omega t})$ are the single-mode field's quadrature components, angle brackets denote quantum averaging, and $\Delta\hat{a}_i(t) \equiv \hat{a}_i(t) - \langle\hat{a}_i(t)\rangle$, for $i = 1, 2$, are their associated fluctuation operators. Moreover these states also have minimum uncertainty sum, i.e., they satisfy $\langle[\Delta\hat{a}_1(t)]^2\rangle = \langle[\Delta\hat{a}_2(t)]^2\rangle = 1/4$ at all times.

The quantum-mechanical single-mode field stands in stark contrast to its classical counterpart. As sketched in Fig. 4, the classical field can, in principle, be a noiseless sinusoid, with a phase-space plot that is a point. The coherent-state quantum field, on the other hand, has non-zero constant standard deviation at all time instants, hence its associated phase-space plot is a circularly symmetric blur, see Fig. 5.
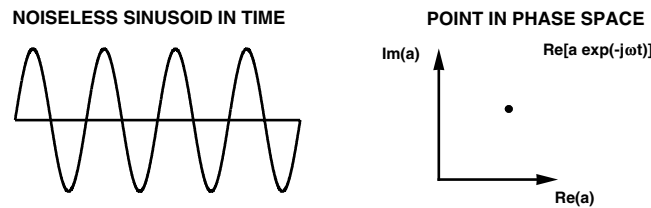

Figure 4. Left: noiseless sinusoid of the ideal single-mode classical field. Right: phase-space point of the ideal single-mode classical field.

The coherent state gives phase-insensitive noise behavior at the Heisenberg uncertainty principle limit. As noted in the previous subsection, the coherent-state field has quantum photodetection statistics that are congruent to those of semiclassical photodetection. There are other minimum-uncertainty states for the quadratures of a single-mode field, states with unequal uncertainties in the two quadratures. These states have phase-sensitive noise, as sketched in Figs. 6 and 7, and are nonclassical, viz., their photodetection statistics cannot be found from semiclassical theory. Because the Heisenberg uncertainty principle sets a lower limit on the area of the
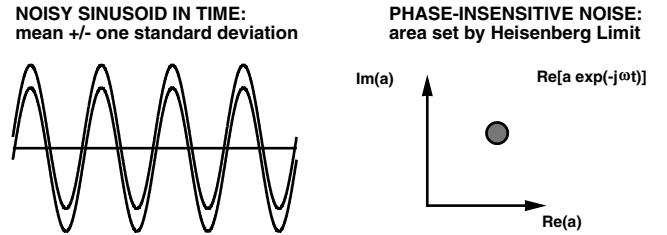
NOISY SINUSOID IN TIME:
mean +/- one standard deviation

PHASE-INSENSITIVE NOISE:
area set by Heisenberg Limit

Im(a)　　　　　Re[a exp(-jωt)]

Re(a)

Figure 5. Left: mean ± one standard deviation time-domain plot of the single-mode, coherent-state quantum field. Right: one-standard-deviation circular phase-space blur of the single-mode, coherent-state quantum field.
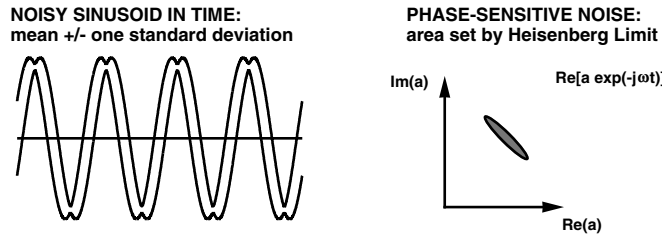
NOISY SINUSOID IN TIME:
mean +/- one standard deviation

PHASE-SENSITIVE NOISE:
area set by Heisenberg Limit

Im(a)　　　　　Re[a exp(-jωt)]

Re(a)

Figure 6. Left: mean ± one standard deviation time-domain plot of the single-mode, amplitude-squeezed quantum field. Right: one-standard-deviation elliptical phase-space blur of the single-mode, amplitude-squeezed quantum field.

one-standard-deviation phase-space plot, phase-sensitive minimum-uncertainty-product states are called squeezed states: the noise squeezed out of one phase angle must appear in the $\pi/2$-rad-shifted quadrature. In Fig. 6 we show an amplitude-squeezed state; its low-noise quadrature is in phase with its mean value, hence its noisy-sinusoid time waveform has greatest accuracy near peaks and troughs of the wave. In Fig. 7 we show a phase-squeezed state; its low-noise quadrature is $\pi/2$-rad shifted from its mean value, hence its noisy-sinusoid time waveform has greatest accuracy near the wave's zero crossings. It is important to note that these states have larger total (sum of quadrature variances) noise than does the coherent state. Nevertheless, because optical homodyne detection permits phase-sensitive optical measurements to be performed, an amplitude-shift-keyed communication system can homodyne detect an amplitude-squeezed light beam and obtain a higher signal-to-noise ratio than that of a coherent-state system with the same average photon number.[20] Likewise, an interferometric optical precision measurement system can use the enhanced zero-crossing sensitivity of the phase-squeezed state to outperform a coherent-state interferometer of the same average photon number.[21]

The squeezed states of the single-mode field—minimum uncertainty-product states for the quadratures with phase-sensitive noise distributions—turn out to be Gaussian states.[22] Describing their generation, via parametric amplification, and surveying the nonclassical effects that they produce in a variety of photodetection configurations comprise the rest of this paper.
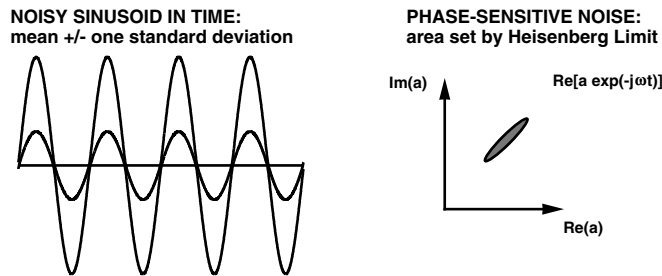
NOISY SINUSOID IN TIME:
mean +/- one standard deviation

PHASE-SENSITIVE NOISE:
area set by Heisenberg Limit

Im(a)　　　　　Re[a exp(-jωt)]

Re(a)

Figure 7. Left: mean ± one standard deviation time-domain plot of the single-mode, phase-squeezed quantum field. Right: one-standard-deviation elliptical phase-space blur of the single-mode, phase-squeezed quantum field.

3. GENERATION OF QUANTUM GAUSSIAN NOISE

In a second-order ($\chi^{(2)}$) nonlinear optical material, such as potassium titanyl phosphate (KTP), three-wave mixing can take place between pump (P), signal (S), and idler (I) beams whose frequencies satisfy the energy-conservation condition, $\omega_P = \omega_S + \omega_I$, and whose wave vectors satisfy the momentum-conservation condition, $\vec{k}_P = \vec{k}_S + \vec{k}_I$.[23] Of interest here is the parametric downconversion form of this interaction, sketched in Fig. 8, in which the only input is the strong pump beam, but weak signal and idler outputs are generated by the three-wave mixing process. When the nonlinear crystal is placed between a pair of mirrors that resonate the signal and idler
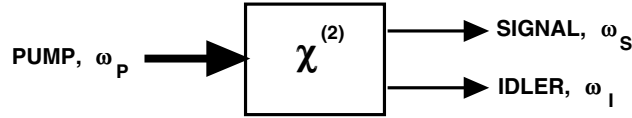

Figure 8. Schematic of parametric downconversion: a strong pump beam at frequency ω_P produces signal and idler fields at frequencies ω_S and ω_I, respectively, via parametric interaction in a $\chi^{(2)}$ nonlinear material.

beams, a strong narrowband interaction results. The resonant signal and idler cavities formed by these mirrors can provide enough positive feedback to drive the system into oscillation, resulting in an optical parametric oscillator (OPO), a device with laser-like characteristics. Our quantum Gaussian noise source, however, will be the sub-threshold OPO, i.e., the optical parametric amplifier (OPA) shown in Fig. 9. In the ideal case—in which
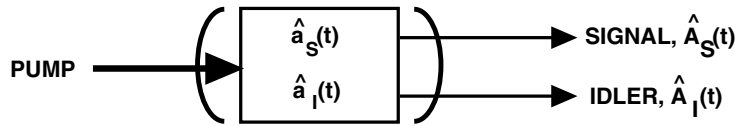

Figure 9. Schematic of the doubly-resonant optical parametric amplifier: the single-ended optical cavity resonates the signal and idler frequencies, but not the pump; $\hat{a}_i(t)$ and $\hat{A}_i(t)e^{-j\omega_i t}$, for $i = S, I$, are the intracavity annihilation operators and external positive-frequency field operators of the signal and idler, respectively.

there is no detuning, no excess noise on the pump, no pump depletion, and no excess losses in the cavities—the internal equations of motion for this doubly-resonant optical parametric amplifier (OPA) take the following form:[24]

$$\left(\frac{\mathrm{d}}{\mathrm{d}t} + \Gamma\right)\hat{a}_i(t) = G\Gamma\hat{a}_k^\dagger(t) + \sqrt{2\Gamma}\hat{A}_i^{\mathrm{IN}}(t), \quad \text{for } i, k = S, I, \, i \neq k. \tag{4}$$

Here: $\hat{a}_S(t)$ and $\hat{a}_I(t)$ are the intracavity annihilation operators of the signal and idler fields; $\hat{A}_S^{\mathrm{IN}}(t)e^{-j\omega_S t}$ and $\hat{A}_I^{\mathrm{IN}}(t)e^{-j\omega_I t}$ are the positive-frequency signal and idler fields at the input to the amplifier; $G^2 = P_P/P_T$ is the normalized OPA gain, where P_P is the pump power and P_T is the oscillation threshold; and Γ is linewidth of the (assumed to be identical) signal and idler cavities. The signal and idler outputs from the OPA are given by:[24]

$$\hat{A}_i(t) = \sqrt{2\Gamma}\hat{a}_i(t) - \hat{A}_i^{\mathrm{IN}}(t), \quad \text{for } i = S, I. \tag{5}$$

For the purpose of generating quantum Gaussian noise, the input signal and idler fields are in their vacuum states. The parametric coupling between the signal and idler, within the OPA cavity, then performs phase-sensitive amplification and attenuation of combinations of the signal and idler fields, leading to nonclassical Gaussian-state outputs. In a photon-based picture, a single pump photon is split into two lower-frequency photons (one signal and one idler) that satisfy the energy and momentum conservation conditions given above. This photon-pair generation process is intrinsically nonclassical, as we shall see below.

Equations 4 and 5 can be used to prove that the OPA produces signal and idler outputs that are in an entangled, zero-mean, Gaussian pure state, and that this state is completely characterized by the following

non-zero normally-ordered and phase-sensitive correlation functions:[17]

$$\langle \hat{A}_i^\dagger(t+\tau)\hat{A}_k(t)\rangle \;\; = \;\; \delta_{ik}\frac{G\Gamma}{2}\left[\frac{e^{-(1-G)\Gamma|\tau|}}{1-G}-\frac{e^{-(1+G)\Gamma|\tau|}}{1+G}\right], \tag{6}$$

$$\langle \hat{A}_i(t+\tau)\hat{A}_k(t)\rangle \;\; = \;\; (1-\delta_{ik})\frac{G\Gamma}{2}\left[\frac{e^{-(1-G)\Gamma|\tau|}}{1-G}+\frac{e^{-(1+G)\Gamma|\tau|}}{1+G}\right], \tag{7}$$

for $i,k = S, I$.

With the preceding joint signal-idler state characterization in hand, we can now provide quantitative descriptions of the nonclassical photodetection effects that can be produced by quantum Gaussian noise. Before doing so, however, let us introduce the classical-field model that comes closest to reproducing the quantum Gaussian noise represented by Eqs. 6 and 7. This model will enable us to contrast purely-quantum photodetection behavior with the limits set by the semiclassical theory. The classical field statistics we need—for use in conjunction with the conditionally-Poisson shot-noise theory of photodetection—are as follows. The (photon-units) signal and idler fields at the output of the OPA are $A_S(t)e^{-j\omega_S t}$ and $A_I(t)e^{-j\omega_I t}$, respectively, where $A_S(t)$ and $A_I(t)$ are zero-mean, jointly-Gaussian, complex-valued, classical random processes which are completely characterized by their non-zero correlation functions,

$$\langle A_i^*(t+\tau)A_k(t)\rangle \;\; = \;\; \delta_{ik}\frac{G\Gamma}{2}\left[\frac{e^{-(1-G)\Gamma|\tau|}}{1-G}-\frac{e^{-(1+G)\Gamma|\tau|}}{1+G}\right], \tag{8}$$

$$\langle A_i(t+\tau)A_k(t)\rangle \;\; = \;\; (1-\delta_{ik})\frac{G\Gamma}{2}\left[\frac{e^{-(1-G)\Gamma|\tau|}}{1-G}-\frac{e^{-(1+G)\Gamma|\tau|}}{1+G}\right], \tag{9}$$

for $i,k = S, I$. Here, angle brackets have been used to denote classical ensemble averaging, to maintain notational similarity to the quantum case.

4. QUANTUM EFFECTS FROM PARAMETRIC AMPLIFIERS

The correlation functions that specify the statistics of the quantum and classical Gaussian-noise models for the optical parametric amplifier are nearly identical, the only difference being the sign between the exponential terms in Eqs. 7 and 9. The origin of this sign difference is that the quantum model involves a field operator, $\hat{E}(t)$, that does not commute with its adjoint, $\hat{E}^\dagger(t)$, whereas the classical model treats a complex-valued field, $E(t)$, whose multiplication by its complex-conjugate, $E^*(t)$, is commutative. Non-zero commutators in quantum mechanics imply Heisenberg uncertainty relations, i.e., the fundamental presence of quantum noise. The photodetection phenomena that we will quantify below derive directly from such quantum noise.

4.1. Quadrature Noise Squeezing

The quadrature components of the photon-units positive-frequency field ($E(t)$ in semiclassical theory, $\hat{E}(t)$ in the quantum theory) can be measured via dual-detection (balanced-mixer) homodyning, as shown in Fig. 10. The field from a strong local-oscillator (LO) laser at frequency ω is combined with that of a weak frequency-ω input field on a 50/50 beam splitter. The output from the beam splitter then illuminates a pair of photodetectors, whose output currents are subtracted to yield a homodyne photocurrent, $i_\theta(t)$, which depends on the phase θ of the continuous-wave LO field. In the semiclassical theory of photodetection we have that,[1,5]

$$i_\theta(t) = 2q\sqrt{P_{\text{LO}}/\hbar\omega}\,A_\theta(t) + i_{\text{LO}}(t), \tag{10}$$

where P_{LO} is the LO power, $\hbar\omega$ is the photon energy at the LO frequency, $A_\theta(t) \equiv \text{Re}[E(t)e^{j(\omega t-\theta)}]$, and $i_{\text{LO}}(t)$ (the LO shot noise) is a zero-mean, stationary, white Gaussian noise with spectrum $q^2 P_{\text{LO}}/\hbar\omega$. In the quantum theory of photodetection, the classical current $i_\theta(t)$ has the same statistics as the quantum measurement,,[4,5]

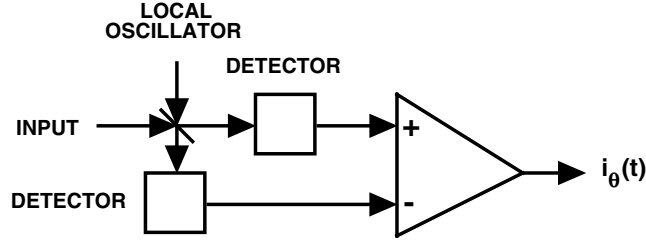$$\hat{i}_\theta(t) = 2q\sqrt{P_{\text{LO}}/\hbar\omega}\,\hat{A}_\theta(t), \tag{11}$$

Figure 10. Schematic of balanced-mixer optical homodyne detection.

where $\hat{A}_\theta(t) \equiv \mathrm{Re}[\hat{E}(t)e^{j(\omega t - \theta)}]$ is the quantum field's baseband quadrature operator at angle θ.

Suppose that we operate our doubly-resonant OPA at frequency degeneracy $\omega_S = \omega_I = \omega$, and homodyne detect the 50/50 combination of the signal and idler fields, $[\hat{E}_S(t) + \hat{E}_I(t)]/\sqrt{2}$ for the quantum case, and $[E_S(t) + E_I(t)]/\sqrt{2}$ for the semiclassical treatment, as shown in Fig. 11. The spectrum of the homodyne output current
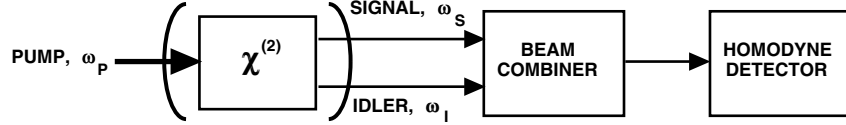

Figure 11. Schematic of quadrature-noise squeezing measurement.

at radio-frequency Ω, normalized by its value for a vacuum-state input (where the quantum and semiclassical theories agree on a white-noise spectrum of level $q^2 P_{\mathrm{LO}}/\hbar\omega$), can be shown to be,[17]

$$S_\theta(\Omega) = \begin{cases} |\mu(\Omega) + \nu(\Omega)e^{-2j\theta}|^2, & \text{quantum theory,} \\ 1 + |\nu(\Omega)|^2|1 + e^{-2j\theta}|^2, & \text{semiclassical theory,} \end{cases} \tag{12}$$

where

$$\mu(\Omega) \equiv \frac{G^2 + \Omega^2/\Gamma^2 + 1}{1 - G^2 - \Omega^2/\Gamma^2 - 2j\Omega/\Gamma}, \tag{13}$$

$$\nu(\Omega) \equiv \frac{2G}{1 - G^2 - \Omega^2/\Gamma^2 - 2j\Omega/\Gamma}. \tag{14}$$

In Fig. 12(a) we have plotted the zero-frequency spectrum value, $S_\theta(0)$, as a function of the local-oscillator phase shift θ for OPA gain $G^2 = 0.1$. In the semiclassical theory, this zero-frequency spectrum is phase sensitive, but it never falls below the LO-shot-noise limit of $q^2 P_{\mathrm{LO}}/\hbar\omega$, i.e., $0\,\mathrm{dB}$ on this normalized-spectrum plot. In the quantum theory, however, the phase-sensitive behavior occurs with a noise minimum that can go well below this shot-noise limit. As discussed in Sec. 2.3, the latter behavior is the signature of a squeezed state. Experiments[7] have shown the sub-shot-noise property of the squeezed-state homodyne photocurrent, confirming the generation of these nonclassical states. Figure 12(b) plots $\min_\theta[S_\theta(\Omega)]$ versus Ω for the quantum theory, viz., the frequency dependence of the quantum homodyne photocurrent's low-noise quadrature, for several values of the OPA gain. Here we see that very substantial noise reductions occur as the gain increases, but they are confined to frequencies within the cavity linewidth of the OPA. Note that $\min_\theta[S_\theta(\Omega)] = 1$ in the semiclassical theory.

4.2. Photon-Twins Generation

Suppose that we operate the OPA in nondegenerate mode, and perform separate T-sec-long photon counting measurements on its signal and idler outputs, see Fig. 13. Because signal and idler photons are created in pairs, within the $\chi^{(2)}$ crystal, and emerge from the ideal-OPA cavity within a few reciprocal cavity-linewidths of one
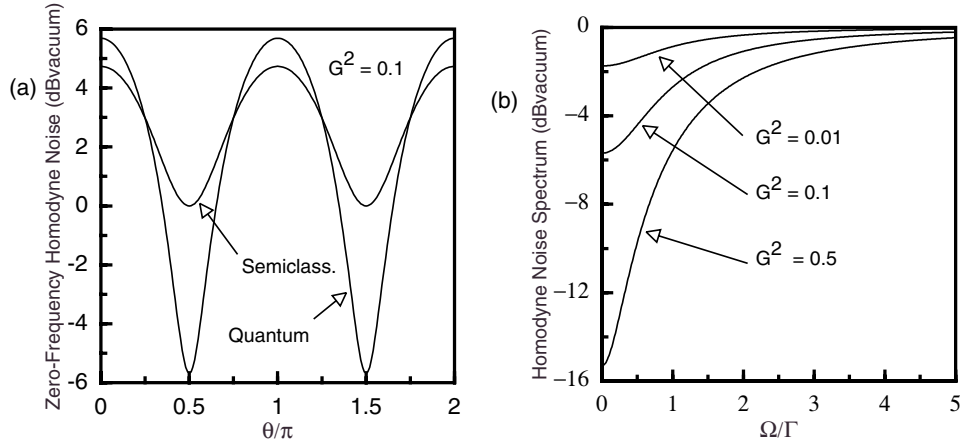
Figure 12. Left (a), normalized zero-frequency homodyne photocurrent spectrum for the quantum and semiclassical models versus LO phase shift θ with $G^2 = 0.1$. Right (b), normalized homodyne photocurrent spectrum for the low-noise quadrature, $\min_\theta[S_\theta(\Omega)]$, versus frequency for various values of the OPA gain; all curves shown are from the quantum theory, because $\min_\theta[S_\theta(\Omega)] = 1$ in the semiclassical theory.
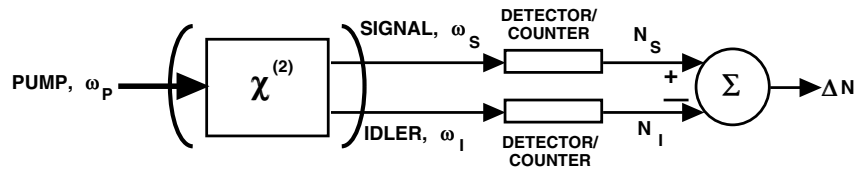

Figure 13. Schematic of photon twin-beam measurement.

another, there should be a strong correlation between the signal-beam photocount, N_S, and the idler-beam photocount, N_I. From our quantum and semiclassical statistical OPA models, we have that,[16, 17]

$$\langle N_S \rangle = \langle N_I \rangle = \frac{G^2 \Gamma T}{1 - G^2}, \quad \text{quantum and semiclassical theories,} \tag{15}$$

specifies the mean values of the signal and idler counts, and

$$\frac{\langle \Delta N^2 \rangle}{\langle N_S \rangle + \langle N_I \rangle} = \begin{cases} \dfrac{1 - e^{-2\Gamma T}}{2\Gamma T}, & \text{quantum theory,} \\ 1, & \text{semiclassical theory,} \end{cases} \tag{16}$$

gives the variance of their difference, normalized to the vacuum-state (shot-noise) level.

In Fig. 14(a) we have plotted the normalized (to vacuum-state level) signal-count variance versus ΓT, the product of the OPA's cavity linewidth and the counting-interval duration, when $G^2 = 0.01$. Both the semiclassical and the quantum theories agree on their predictions for this single-beam statistic, because the signal field alone is in a classical state, i.e., a classically-random mixture of coherent states.[17] The signal and idler beams are entangled in the quantum theory, viz., whenever there is a signal photon there is an accompanying idler photon, because they are simultaneously created from annihilation of a single pump photon. This entanglement can be seen in Eq. 16: when the counting interval is much longer than the reciprocal cavity-linewidth ($\Gamma T \gg 1$) the normalized count-difference variance is approximately $1/2\Gamma T$, in the quantum theory, which is far below the unity-value of the semiclassical shot-noise limit, as shown in Fig. 14(b). The above-threshold (optical parametric oscillator) version of this nonclassical photon-twins behavior has been seen experimentally,[8] confirming another nonclassical aspect of the quantum Gaussian noise produced by parametric interactions.
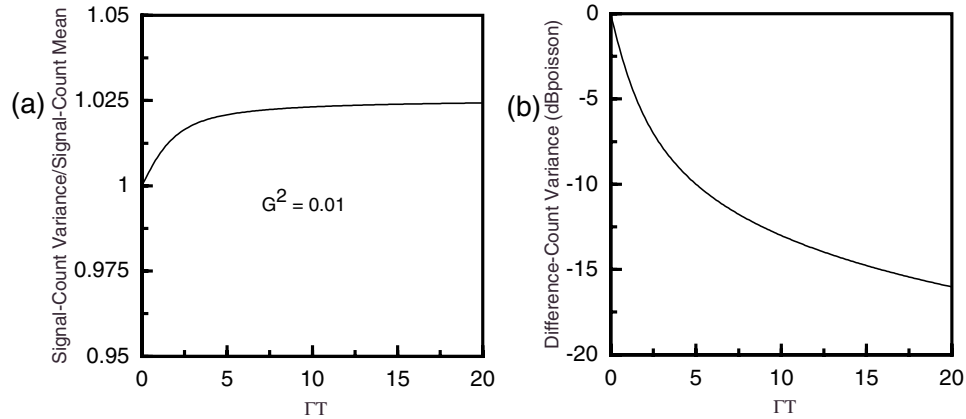
Figure 14. Left (a), variance of the signal count normalized by its mean (the vacuum-state noise level) versus ΓT when $G^2 = 0.01$; the quantum and semiclassical theories have identical predictions for this statistic. Right (b), variance of the photocount difference normalized by the vacuum-state (shot-noise) level in the quantum theory; this statistic is independent of the OPA gain.
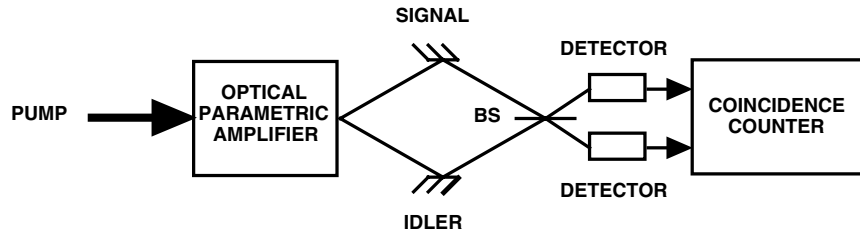

Figure 15. Schematic of nonclassical fourth-order interference experiment.

4.3. Nonclassical Fourth-Order Interference

When the signal and idler outputs from a degenerate ($\omega_S = \omega_I = \omega$) OPA are used as the inputs to the arrangement shown in Fig. 15, an interference pattern that is of fourth order in the optical field is traced out as the differential delay, T, between the two paths is changed by moving the central beam splitter up and down. Each detector/counter in this figure uses a T_c-sec counting interval that is much longer than the reciprocal cavity-linewidth of the OPA, and the OPA gain is kept low enough that the probability of more than one photon pair being present within any T_c-sec-long interval is negligible.

The signal and idler photons that originate from annihilation of a particular pump photon within the degenerate OPA are indistinguishable. If this pair arrives simultaneously at the beam splitter in Fig. 15, their indistinguishability leads to a quantum cancellation such that both photons must exit from the same beam splitter port, hence there will never be a coincidence count, i.e., the two photon counters will never increment within the same T_c-sec interval. On the other hand, when the differential delay between the two paths exceeds a few reciprocal linewidths of the OPA cavity, the signal and idler photons arriving at the beam splitter are distinguishable, hence coincidence counts are possible. Indeed, the coincidence probability will then approach the single-detector count probability, in the quantum theory, because of the entanglement between the signal and idler. Note that there is never any second-order interference in this setup, i.e., the individual count rates on each detector are independent of the differential-delay setting, T.

Figures 16(a) and 16(b) plot the semiclassical and quantum theories, calculated via the technique used in Ref. 17 for the coincidence rate (average number of coincidences per T_c-sec-interval) normalized by the singles rate (average number of signal counts per T_c-sec-interval) versus ΓT, the differential delay measured in units of the OPA cavity lifetime, with $\Gamma T_c = 100$ and $G^2 = 10^{-5}$. We see that the semiclassical theory predicts a coincidence rate that is very much smaller than the singles rate, with a nearly imperceptible dip occurring at
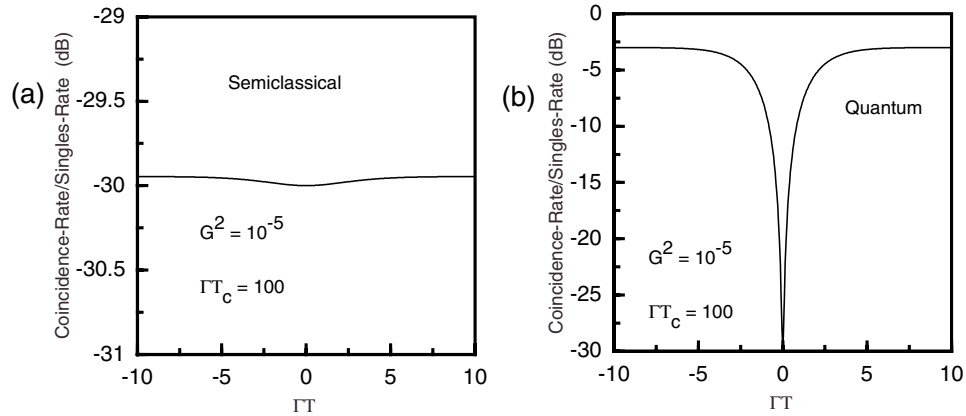
Figure 16. Signal-idler coincidence rate normalized by the signal-beam singles rate versus ΓT, with $G^2 = 10^{-5}$ and $\Gamma T_c = 100$. Left (a), semiclassical theory. Right (b), quantum theory.

$T = 0$. The quantum theory, however, shows a coincidence rate that is within a few dB of the singles rate, except for a pronounced fourth-order cancellation at $T = 0$. The parametric downconverter (nonresonant) version of this experiment has been performed;[9] its results confirm the validity of the quantum theory.

4.4. Polarization-Entangled Photon Pairs

Polarization entanglement lies at the core of recent experiments in quantum teleportation.[25, 26] The state of a single photon can, in general, be an arbitrary superposition $|\psi\rangle = \alpha|\uparrow\rangle + \beta|\bullet\rangle$ of two orthogonal polarization states, $|\uparrow\rangle$, and $|\bullet\rangle$, where $|\alpha|^2 + |\beta|^2 = 1$. The singlet state of two polarization-entangled photons is then expressible as,

$$|\psi\rangle_{12} = (|\uparrow\rangle_1|\bullet\rangle_2 - |\bullet\rangle_1|\uparrow\rangle_2)/\sqrt{2}, \tag{17}$$

where for each ket $|\cdot\rangle_i$ on the right the subscript denotes the photon (1 or 2) whose polarization is being specified by the content of that ket. This is an entangled state because the polarization of either photon is completely random, yet, given that the polarization of photon 1 is specified by a particular 2-D complex-valued unit vector $\vec{\mathbf{i}}$, then there is a definite, conjugate polarization, specified by another 2-D complex-valued unit vector $\vec{\mathbf{i}}'$, that the second photon must have. For example, if the first photon is $\uparrow$, then the second photon must be $\bullet$, etc.
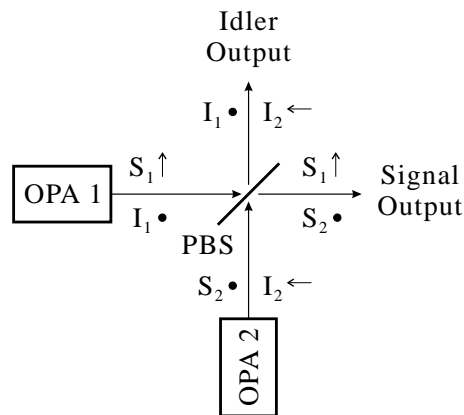

Figure 17. Type-II OPA configuration for generating polarization-entangled photon pairs. For each optical beam, the propagation direction is $\hat{z}$, and $\hat{x}$ and $\hat{y}$ polarizations are denoted by arrows and bullets, respectively. PBS: polarizing beam splitter.
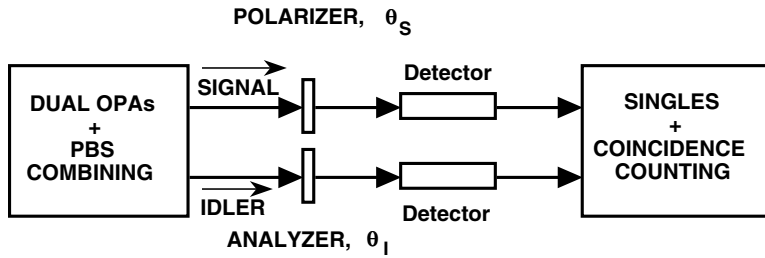
Figure 18. Schematic of polarization-entanglement measurement setup.

Polarization-entangled photon pairs can be produced by a pair of OPAs,[16] using the arrangement shown in Fig. 17. Each OPA is type-II phase matched, hence its output signal and idler beams are orthogonally polarized. By employing a π-rad phase shift between the pump beams for these two OPAs and combining their respective outputs on a polarizing beam splitter we generate vector signal and idler beams that are polarization entangled with signal-idler photon pairs that are in singlet states. As in the photon-twins and the fourth-order interference experiments, the two photons of any particular signal-idler pair are time coincident to within a few reciprocal linewidths of the OPA cavity.
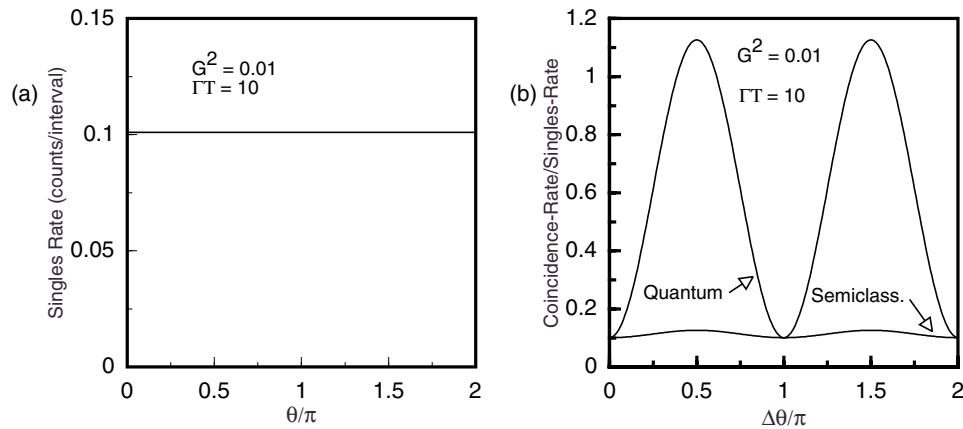

Figure 19. Left (a), signal-beam singles rate (counts per T-sec-interval) versus polarizer angle $\theta_S = \theta$ for $G^2 = 0.01$ and $\Gamma T = 10$; the idler-beam singles rate versus $\theta_I = \theta$ is identical to this signal-beam plot. Right (b), signal-idler coincidence rate (coincidences per T-sec-interval), normalized by the (signal or idler) singles rate, versus $\Delta\theta \equiv \theta_S - \theta_I$ with $G^2 = 0.01$, $\Gamma T = 10$.

If we pass the vector signal field through a polarizer set at angle θ_S and the vector idler field through an analyzer set at angle θ_I, as shown in Fig. 18, we can exhibit their polarization entanglement via T-sec-long photon-counting measurements, with $\Gamma T \gg 1$, by comparing the resulting singles and coincidence rates as the difference angle, $\Delta\theta \equiv \theta_S - \theta_I$, is varied. It turns out that the signal-beam and idler-beam counting measurements have identical singles rates that are independent of θ_S and θ_I, see Fig. 19(a), in keeping with the statement that the individual photons from a polarization-entangled pair are in states of completely random polarization. When the OPA gain is low enough that there is negligible probability of more than one signal-idler pair occurring within a T-sec-long interval, the approach taken in Ref. 17 can be used to show that the quantum and semiclassical coincidence rates have very different behavior. As shown in Fig. 19(b), the semiclassical coincidence rate is approximately equal to the product of the signal and idler singles rates, with a weak sinusoidal fringe whose peaks occur when θ_S and θ_I are set at conjugate polarizations, $\Delta\theta = (2m + 1)\pi/2$ for $m = 0, 1$. The quantum coincidence rate, however, shows a strong sinusoidal fringe whose peak greatly exceeds the product of the singles rates. The parametric downconverter (non-resonant parametric interaction) version of this experiment has been performed;[10] its results confirm the quantum-theory prediction for this our last quantum Gaussian noise example.

5. CONCLUSION

We have taken a rapid walk through the field of quantum Gaussian noise. High-sensitivity photodetection systems are limited by noise of quantum-mechanical origin, and nonclassical light can lead to photodetection statistics that cannot be predicted by the standard, conditional Poisson-process model of semiclassical theory. The quantum Gaussian noise we have discussed has a variety of potential applications, and it is an area of continuing experimental and theoretical research.

ACKNOWLEDGMENTS

REFERENCES

1. R. M. Gagliardi and S. Karp, *Optical Communications*, Wiley, New York (1976).
2. B. E. A. Saleh, *Photoelectron Statistics*, Springer-Verlag, Berlin (1978).
3. L. Mandel and E. Wolf, *Optical Coherence and Quantum Optics*, Cambridge University Press, Cambridge (1995), chapter 9.
4. H. P. Yuen and J. H. Shapiro, "Optical communication with two-photon coherent states—part III: quantum measurements realizable with photoemissive detectors," IEEE Trans. Inform. Theory **26**, 78 (1980).
5. J. H. Shapiro, "Quantum noise and excess noise in optical homodyne and heterodyne receivers," IEEE J. Quantum Electron. **21**, 237 (1985).
6. R. J. Glauber, "Optical coherence and photon statistics," in *Quantum Optics and Electronics*. C. DeWitt *et al.*, eds., Gordon and Breach, New York (1965).
7. L.-A. Wu, H. J. Kimble, J. L. Hall, and H. Wu, "Generation of squeezed states by parametric downconversion," Phys. Rev. Lett. **57** 2520 (1986).
8. A. Heidmann, R. J Horowicz, S. Reynaud, E. Giacobino, C. Fabre, and G. Camy, "Observation of quantum noise reduction on twin laser beams," Phys. Rev. Lett. **59**, 2555 (1987).
9. R. Ghosh and L. Mandel, "Observation of nonclassical effects in the interference of two photons," Phys. Rev. Lett. **59** 1903 (1987).
10. P. G. Kwiat, K. Mattle, H. Weinfurter, A. Zeilinger, A. V. Sergienko, and Y. Shih, "New high-intensity source of polarization-entangled photon pairs," Phys. Rev. Lett. **75**, 4337 (1995).
11. J. H. Shapiro, "Optical waveguide tap with infinitesimal insertion loss," Opt. Lett. **5** 351 (1980).
12. C. M. Caves, "Quantum-mechanical noise in an interferometer," Phys. Rev. D **23**, 1693 (1981).
13. A. K. Ekert, "Quantum cryptography based on Bell's theorem," Phys. Rev. Lett. **67**, 661 (1991).
14. C. H. Bennett, G. Brassard, C. Crépeau, R. Jozsa, A. Peres, and W. K. Wootters, "Teleporting an unknown quantum state via dual classical and Einstein-Podolsky-Rosen channels," Phys. Rev. Lett. **70**, 1895 (1993).
15. S. L. Braunstein and H. J. Kimble, "Teleportation of continuous quantum variables," Phys. Rev. Lett. **80**, 869 (1998).
16. J. H. Shapiro and N. C. Wong, "An ultrabright narrowband source of polarization-entangled photon pairs," J. Opt. B: Quantum Semiclass. Opt. **2**, L1 (2000).
17. J. H. Shapiro and K.-X. Sun, "Semiclassical versus quantum behavior in fourth-order interference," J. Opt. Soc. Am. B **11**, 1130 (1994).
18. D. L. Snyder, *Random Point Processes*, Wiley, New York (1975).
19. W. H. Louisell, *Quantum Statistical Properties of Radiation*, McGraw-Hill, New York (1973), chapter 1.
20. H. P. Yuen and J. H. Shapiro, "Optical communication with two-photon coherent states—part I: quantum state propagation and quantum noise reduction," IEEE Trans. Inform. Theory **IT-24**, 657 (1978).
21. R. S. Bondurant and J. H. Shapiro, "Squeezed states in phase-sensing interferometers," Phys. Rev. D **30**, 2548 (1984).
22. H. P. Yuen, "Two-photon coherent states of the radiation field," Phys. Rev. A **13**, 2226 (1976).
23. Y. R. Shen, *The Principles of Nonlinear Optics*, Wiley, New York (1984), chapter 9.

24. N. C. Wong, K. W. Leong, and J. H. Shapiro, "Quantum correlation and absorption spectroscopy in an optical parametric oscillator in the presence of pump noise," Opt. Lett. **15**, 891 (1990).

25. D. Bouwmeester, J.-W. Pan, K. Mattle, M. Eibl, H. Weinfurter, and A. Zeilinger, "Experimental quantum teleportation," Nature **390**, 575 (1997).

26. D. Bouwmeester, K. Mattle, J.-W. Pan, H. Weinfurter, A. Zeilinger, and M. Zukowski, "Experimental quantum teleportation of arbitrary quantum states," Appl. Phys. B **67**, 749 (1998).